

Meteorology Group, Department de Física, Universitat de les Illes Balears, Palma de Mallorca, Spain

Performance of two Cumulus Convection Parameterizations for two Heavy Precipitation Events in the Western Mediterranean

R. Romero, C. Ramis, and S. Alonso

With 21 Figures

Received October 10, 1997

Revised February 16, 1998

Summary

A set of mesoscale numerical simulations using the Emanuel and Kain-Fritsch deep convection schemes has been performed in order to determine the sensitivity of the forecast – especially, the rainfall – to the scheme used. The study is carried out for two cases of heavy precipitation in the coastal zone of the Western Mediterranean, where the topographic forcing is of primary influence. The first one, characterized by an almost stationary synoptic situation, is dominated by warm, moist advection at low levels; the second one, of frontal type, presents a much stronger dynamic forcing at upper levels. Although the comparison attempt is conditioned by the limited number of considered cases, the numerical results provide at least some preliminary conclusions. The inclusion of a convective scheme improves the forecast precipitation, through two actions: directly, producing more realistic rainfall patterns in areas of convection; indirectly, avoiding excessive precipitation in areas with orographic or dynamical upward forcing by drying and stabilizing the atmosphere upstream. In particular, the Kain-Fritsch scheme seems to be more sensitive to the orographic forcing, in agreement with observations.

1. Introduction

Attending to its frequent occurrence and hazardous consequences, heavy precipitation is the most serious weather phenomenon that affects the western Mediterranean region (depicted in Fig. 1). As extraordinary records, more than 200 mm in 2 hours were registered in Ibiza

(Balearic Islands) on 15 November 1985 (Ramis et al., 1986), 305 mm in 24 hours in Banyuls sur Mer (southern France) on 3 October 1987 (Ramis et al., 1994), and more than 800 mm in 24 hours in Gandía (Valencia) on 3 November 1987 (Fernández et al., 1995). But many other examples occur every year in coastal regions of Spain, France and Italy, particularly during the autumn season when the Mediterranean sea is quite warm. Font (1983) shows that daily rainfalls exceeding 200 mm have been recorded at most of the observatories of Catalonia and Valencia regions (Fig. 1).

Riosalido (1990) has shown that most of the heavy rainfall events in this area are produced by quasistationary Mesoscale Convective Systems (MCS), although they typically are relatively small in size and practically never fulfill the criteria for a Mesoscale Convective Complex (MCC) given by Maddox (1980). Several Spanish heavy rainfall cases studied in recent works (Ramis et al., 1994; Ramis et al., 1995; Doswell et al., 1998 (hereinafter referred to as DRRA98)), including those considered in this paper, shared, in the zone affected by heavy precipitation, a common synoptic scenario favorable for convection development and its maintenance: moisture convergence in the lowest 1500 metres, upward quasi-geostrophic forcing at 850 hPa, convective

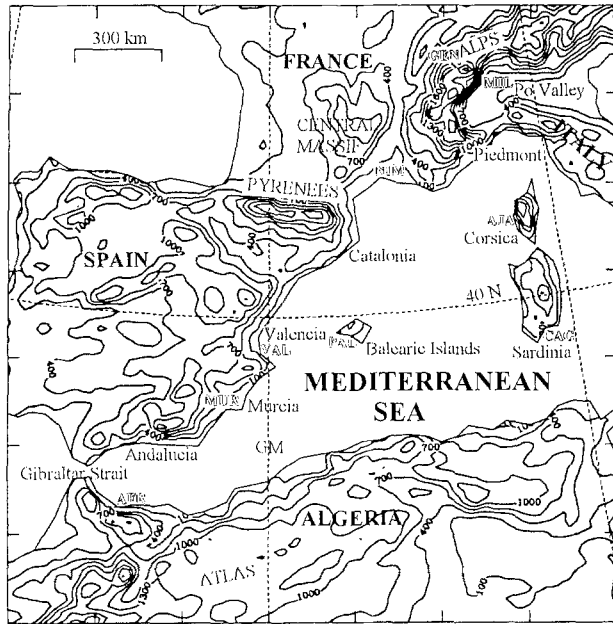


Fig. 1. The western Mediterranean region and its orography (contour interval in 300 m starting at 100 m). The sites mentioned in the text are indicated

instability in the 500–1000 hPa layer, and high values and/or sharp gradients of Convective Available Potential Energy (CAPE). In addition, the important topography that surrounds the Mediterranean basin (notably, the Alps, Pyrenees and Atlas Range; see Fig. 1) plays a decisive role by organizing the low-level flow and focusing convection in coastal areas, as has been shown in a numerical study of a heavy rain event in Catalonia (Romero et al., 1997).

The feasibility of numerical simulations for heavy rain events in the western Mediterranean has been already demonstrated by, among others, Paccagnella et al. (1992) for a heavy rain event in the Po valley, Fernández et al. (1995) for a case occurred in Valencia, Romero et al. (1997) for a case in Catalonia, and Romero et al. (1998) hereinafter referred to as RRADS98 for recent episodes in Valencia, Balearic Islands and Piedmont area (Fig. 1).

Of course, at the resolutions of those numerical simulations (typically, grid lengths of 20 km), the use of some type of convective parameterization scheme seems still necessary since moist convective processes in the atmosphere occur almost exclusively on spatial

scales smaller than those explicitly resolved. Based on different assumptions, several techniques for estimating the rate of subgrid scale convective precipitation and the redistribution of heat, moisture and momentum produced by the ensembles of convective clouds have been developed to be used in numerical models (Frank, 1983). In this work we consider two of the most recent schemes among those techniques and apply them in the simulation of two heavy rainfall cases that occurred in the western Mediterranean. One of the schemes (Emanuel, 1991) assumes the existence of a state of quasi-equilibrium between the rate of large scale atmospheric destabilization and the rate of stabilization by the convective processes, and the second one (Kain and Fritsch, 1990) relies on the local CAPE. In addition, the trigger mechanisms are different in both schemes.

We intend to evaluate how well each scheme performs for the two considered events, which are quite representative of this Mediterranean phenomenology. The relevance of the physical processes involved in the formulation of the convection vary in space and time and its isolation becomes unpractical. Therefore, our work overpass this point and it is essentially practical. The results are intercompared and evaluated by comparison against observed precipitation and thermodynamic vertical profiles, using also information inferred from satellite images.

The simulated events (hereinafter referred to as ‘Algeria’ and ‘Piedmont’ cases) were extensively discussed in DRRA98 from a diagnostic perspective. A complementary approach was used in RRADS98, in which both episodes were reasonably well simulated using a mesoscale model including the convection scheme of Emanuel (1991). It is convenient, however, to provide a short summary of the main results obtained in DRRA98 and RRADS98. This is done in next section. A general presentation of the mesoscale numerical model and a more precise one of the convective schemes under consideration are subject of section 3 and 4 respectively. After the experiments description (section 5), the comparative discussion of the numerical results is presented (section 6 focusing on the precipitation pattern, and section 7 on the atmospheric vertical structure). Finally, section 8 contains the conclusions.

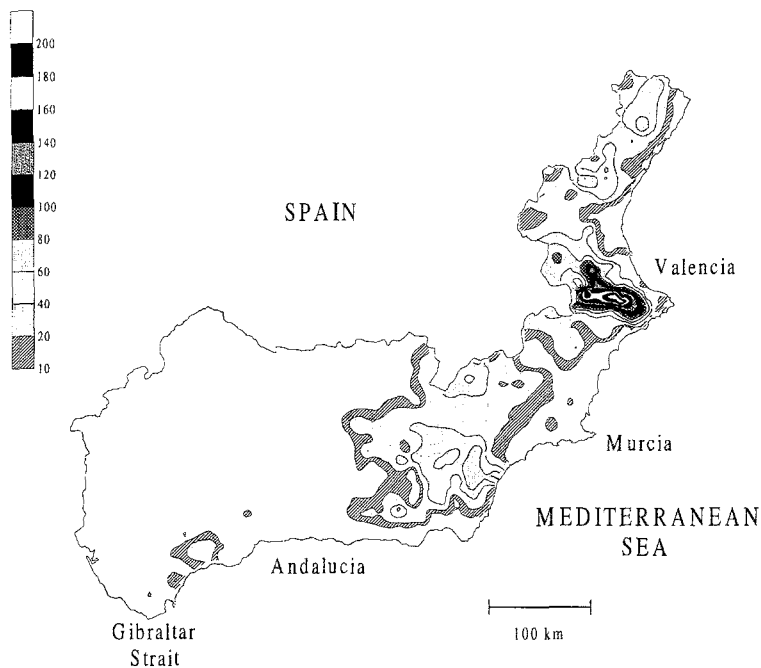
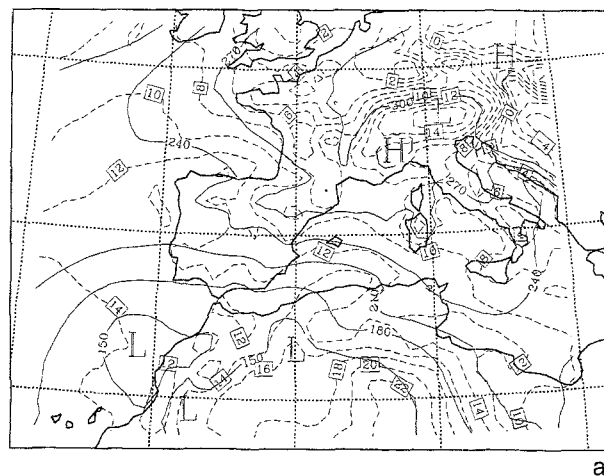


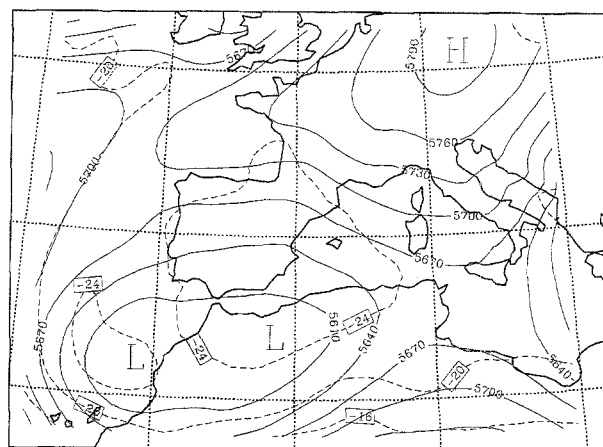
Fig. 2. Accumulated precipitation (mm) in eastern and southern Spain, from 07 UTC on 1 February to 07 UTC on 2 February 1993

2. Events

For the Algeria event, the heavy precipitation occurred over an extended period (1–7 February 1993), and affected eastern and southern Spain. Figure 2 shows the accumulated 24 h. rainfall on the selected day for this study (1 February). That precipitation analysis is similar for the other days of the episode (except on 5 February when little precipitation occurred), showing important local amounts in the Valencia region. Although the situation is unusual in that it occurred during the heart of winter when the sea is colder (most Mediterranean heavy rainfalls happen during the autumn; Font, 1983), the basic synoptic situation became very efficient due to its stationarity. A low-level cyclone was present in northern Africa (Algeria) through much of the period, producing warm advection over the western Mediterranean and allowing the air to charge with moisture through its long and persistent path over the sea (Fig. 3a). At middle and upper levels, a low was located in the south of the Iberian peninsula, exhibiting a structure with two centres (Fig. 3b). A sequence of potential vorticity maps at 300 hPa (not shown) reveals that these two centres were rotating about one another contributing to the stationarity of the system as a whole. A significant feature of this episode was the existence of a deep vertical column of high relative humidity along the eastern coast of



a



b

Fig. 3. Synoptic situation on 2 February 1993 at 00 UTC from ECMWF analyses. (a) 1000 hPa, (b) 500 hPa. Isohypsies (solid line) and isotherms (dashed) are represented

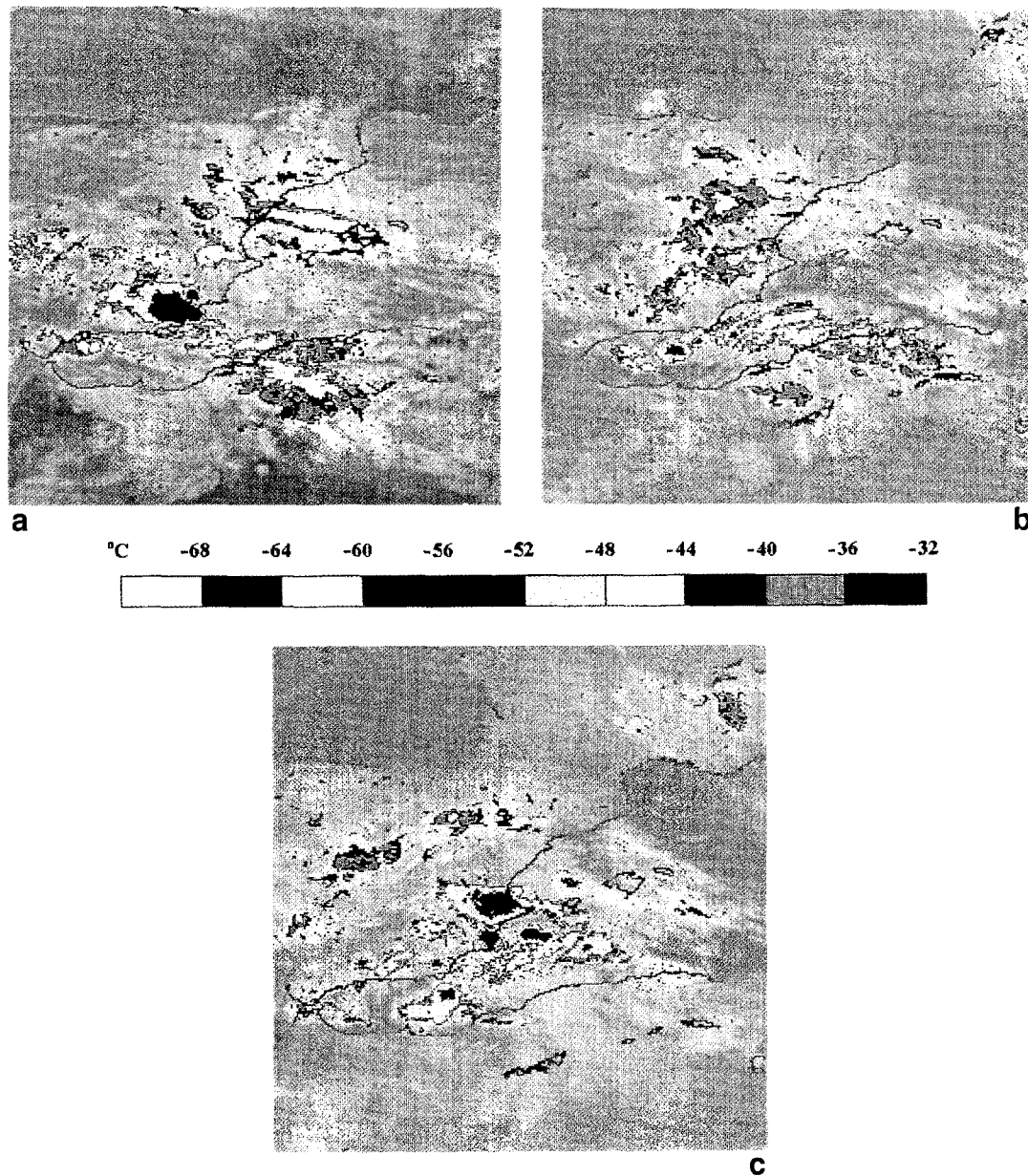


Fig. 4. IR Meteosat images. (a) for 1 February 1993 at 12 UTC, (b) for 1 February 1993 at 20 UTC, (c) for 2 February 1993 at 04 UTC

Spain, supporting the few and geographically confined convective cells responsible for the heavy precipitation (see Fig. 4). Quasigeostrophic forcing for upward motion was weak and mainly controlled by the low-level thermal advection. Rather, the key influence for the convective activity along the coast pertained to

the mesoscale, and was exerted by the orographic lifting on the impinging easterly moist flow. The leading action of this factor was emphasized by the numerical simulations which systematically showed a high correlation between the upslope motion (see Fig. 5 for the first stage of the event), and the observed precipitation (Fig. 2).

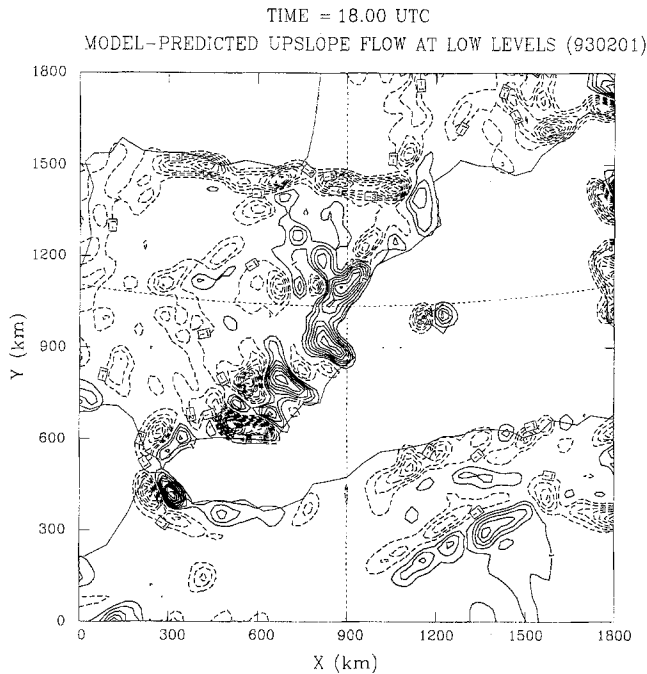


Fig. 5. Forecast upslope flow ($= \vec{V}_s \cdot \vec{\nabla}h$, \vec{V}_s surface wind, h orography) on 1 February 1993 at 18 UTC (simulation starting at 00 UTC, from RRADS98). Solid and dashed lines indicate upward and downward motion respectively. Contour interval is 1 cm s^{-1} starting at 1 and -1 cm s^{-1} .

The Piedmont case (4–6 November 1994) is well known due to the devastating floods that occurred in the Piedmont region (northwestern Italy). Total maximum amounts of precipitation exceeded 500 mm close to the Alps. On 5 November (day selected for our study), the observed precipitation (Fig. 6) shows a tongue structure (up to 250 mm at some points) extending from the coast toward the north along the western part of Italy, and smaller amounts west of this tongue over France and in Corsica and Sardinia. This is an interesting case from the point of view that a significant portion of the rainfall over land appears to be non-convective. Satellite images showed, however, that convection activity affected the coastal area, wide areas of the western Mediterranean sea, and Corsica and Sardinia (Fig. 7). The synoptic pattern was different than that in the previous case, since a cold front associated with a deep trough (Fig. 8) crossed the western Mediterranean. The evolution in the middle and upper troposphere was quite substantial, as a strong jet streak moved through the base of the trough and the trough overall lifted out to the east-northeast. The zone

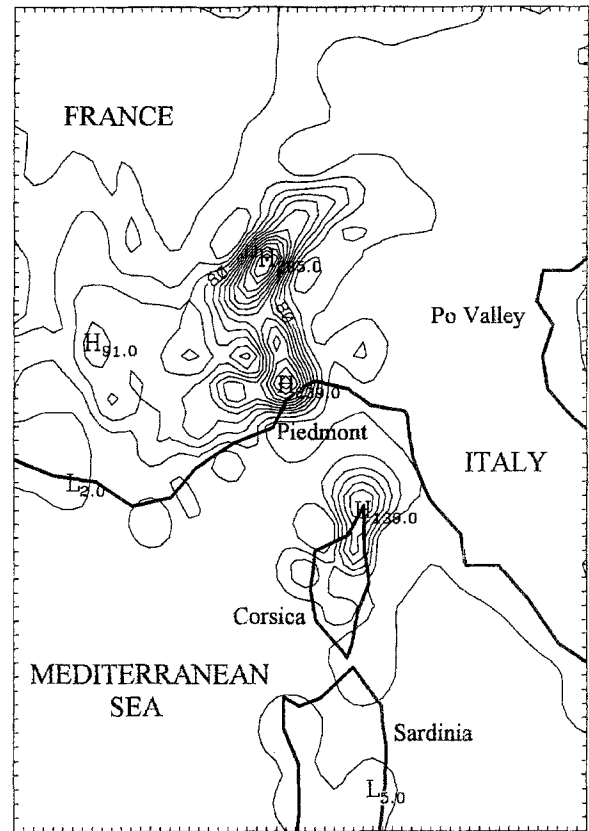


Fig. 6. Analysis of the accumulated precipitation (mm) in the Piedmont area, Corsica and Sardinia (Fig. 1), from 00 UTC to 24 UTC on 5 November 1994. Contour interval is 20 mm starting at 20 mm. (Courtesy of A. Buzzi)



Fig. 7. IR Meteosat image for 5 November 1994 at 18 UTC

of synoptic scale upward forcing at middle and upper levels passed over the Piedmont region during the day of 5 November, enhancing the substantial upslope component provided by the

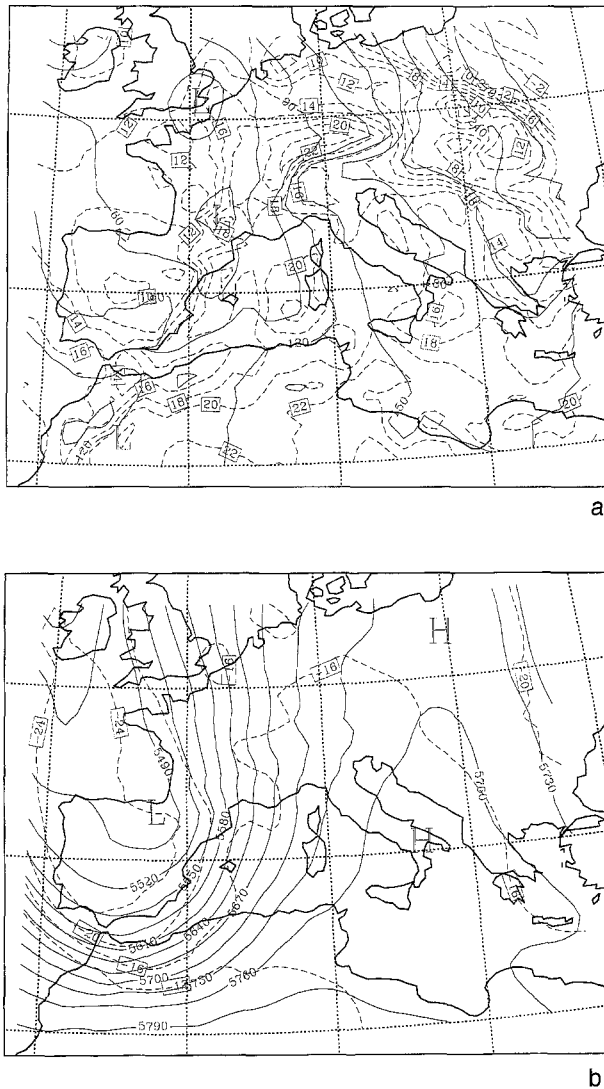


Fig. 8. Synoptic situation on 5 November 1994 at 00 UTC from ECMWF analyses. (a) 1000 hPa, (b) 500 hPa. Isohypsers (solid line) and isotherms (dashed) are represented

southerly flow over the foothills of the Alps in the Piedmont area (Fig. 9).

3. Mesoscale Numerical Model

The meso- β numerical model initially developed by Nickerson et al. (1986) has been used to perform the simulations. The model, hydrostatic, is formulated in a terrain-following coordinates system and has shown its ability to simulate a wide range of mesoscale circulations. For example, mesoscale flows induced by vegetation or soil moisture inhomogeneities (Mahfouf et al., 1987a; Pinty et al., 1989), downslope wind-

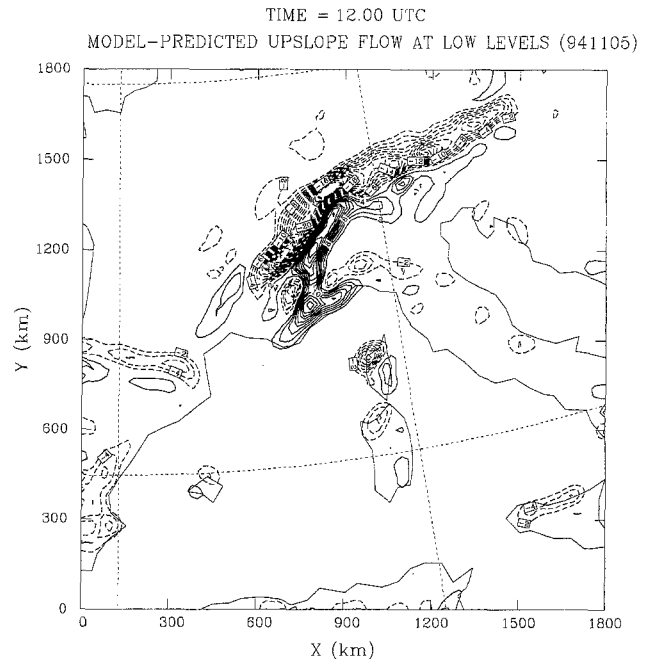


Fig. 9. Forecast upslope flow ($= \vec{V}_s \cdot \vec{\nabla}h$, \vec{V}_s surface wind, h orography) on 5 November 1994 at 12 UTC (simulation starting on 4 November at 18 UTC, from RRADS98). Solid and dashed lines indicate upward and downward motion respectively. Contour interval is 2 cm s^{-1} starting at 2 and -2 cm s^{-1}

storms (Richard et al., 1989), mountain waves (Nickerson et al., 1986; Romero et al., 1995), the breeze circulation (in Florida, Mahfouf et al., 1987b; in Mallorca, Ramis and Romero, 1995), and heavy rain episodes in the Western Mediterranean (Romero et al., 1997; RRADS98)

Resolvable-scale rain is predicted following the parameterization described in Nickerson et al. (1986). This parameterization is based on the work of Berry and Reinhardt (1973) and therefore processes involving ice are not considered. This fact can limit partially the validity of our findings.

Horizontal diffusion is explicit, given by a second-order operator. The vertical turbulent mixing is expressed through an eddy-diffusivity assumption with a 3/2 order closure: the exchange coefficients are calculated as functions of the turbulent kinetic energy (one of the model prognostic variables), and the mixing length scale following the parameterization of Bougeault and Lacarrère (1989).

At the surface, turbulent fluxes of momentum, heat and moisture are calculated following the

parameterization of Louis (1979). The fluxes vary in response to the atmospheric conditions and ground temperature, which is resolved applying the well-known force-restore method (Bhumralkar, 1975; Blackadar, 1976). Available moisture for evaporation is kept constant during the simulation, as well as the albedo, emissivity, roughness and thermal inertia. As in Benjamin and Carlson (1985), all these parameters are given by a single surface index under the assumption that they appear related for natural surfaces. The necessary solar and infrared fluxes are calculated based on Mahrer and Pielke (1977).

In order to minimize reflection from the upper boundary, where the vertical velocity is set to zero, an absorbing layer is included in which the background diffusion is progressively increased with height, reaching its maximum value at the uppermost level. At the lateral boundaries, the method of Davies (1976) is applied to relax the interior fields to the externally specified boundary values.

4. Cumulus Convection Parameterizations

The cumulus convection scheme of Emanuel (1991), hereinafter referred to as EM, is based on the dynamics and microphysics of convection as revealed by aircraft observations. The fundamental entities for moist convective transports are the subcloud-scale drafts rather than the clouds themselves. As opposed to other schemes based on bulk-entraining plumes (e.g., Fritsch and Chappell, 1980; Arakawa and Schubert, 1974), the convective transports are idealized based on reversible ascent of the subcloud-scale entities, mixing, and buoyancy sorting (Raymond and Blyth, 1986). That is, air from the subcloud layer is lifted to each level i between cloud base and the level of neutral buoyancy for undilute air; a fraction of the condensed water is then converted to precipitation, which falls and partially or completely evaporates in an unsaturated downdraft; the remaining cloudy air is then assumed to form a uniform spectrum of mixtures with environmental air at that level, that ascend or descend according to their buoyancy. The EM scheme calculates the updraft mass fluxes of undilute boundary-layer air to each level i (that must be known to close the system) as vertical

velocities determined by the amount of CAPE for undilute ascent to level i , multiplied by fractional areas. These fractional areas are in turn determined in such a way as to drive the mass fluxes toward a state of quasi-equilibrium with the large-scale (explicitly resolved) forcing. A detailed formulation of the scheme can be found in Emanuel (1991).

Alternatively, other authors suggest that the magnitude of convective heating and drying effects on scales less than 50 km (typical resolutions of mesoscale models) is much more strongly correlated with local CAPE than with the large-scale rate of destabilization or moisture convergence (Fritsch et al., 1976; Kreitzberg and Perkey, 1976). Built in basis of this argument, the Kain-Fritsch convective scheme (Kain and Fritsch, 1990), hereinafter referred to as KF, assumes that moist convection only occurs when potential buoyant energy ($PBE \equiv CAPE$) becomes available (ABE), which means that any negative buoyancy experienced by a parcel to rise to its level of free convection has been eliminated or overcome. With this philosophy, convection responds not only to the rate at which the large scale is generating buoyant energy, but also to the buoyant energy generated and stored prior to the onset of deep convection. Processes as low-level convergence, air mass overrunning, or when low-level heating and mixing remove any stable layers drive the atmosphere to the release of convection (PBE becomes ABE). The amount of convection is determined by expanding the stabilization rate (destruction of ABE) over a characteristic short time (30 min–1 h) (Fritsch and Chappell, 1980). The interaction between cloudy parcels and their environment is formulated using a one-dimensional entraining/detraining plume model (see Kain and Fritsch (1990) for a detailed description).

5. Experiments

Numerical simulations of the Algeria and Piedmont events focus on a single day for each case: 1 February 1993 and 5 November 1994 respectively. Given that the available rainfall records from the Spanish rain gauge mesh, used to assess the model results, correspond to daily intervals from 07 to 07 UTC, simulations of the Algeria case (abbreviated as ALG), extend from

Table 1. *Summary of the Numerical Simulations*

	Algeria Case	Piedmont Case
No Convection	ALG/NC	PIE/NC
Emanuel	ALG/EM	PIE/EM
Kain-Fritsch	ALG/KF	PIE/KF

00 UTC on 1 February to 06 UTC on 2 February. They start some hours in advance in order to reduce the spinup influences on the precipitation field during the comparison period. Analogously, simulations of the Piedmont case (abbreviated as PIE) extend from 18 UTC on 4 November to 00 UTC on 6 November since the French and Italian rainfall data are valid for the 00–24 UTC time interval.

Table 1 specifies the characteristics of the experiments performed. Experiments ALG/NC and PIE/NC serve as control or basic experiments since no convection scheme is used. The effects of using each convection parameterization (EM and KF) is determined through experiments ALG/EM and PIE/EM, and ALG/KF and PIE/KF. The few external parameters of the convective schemes have been given the default values suggested by the authors, so that no special tuning of the schemes has been considered.

Working with a polar-stereographic map projection, the resolution is fixed for all experiments to a horizontal grid-length of 20 km and 30 vertical levels. The numerical domain covers $1800 \times 1800 \text{ km}^2$ (91×91 grid points). It is centered at (0°E , 39°N) for ALG simulations and at (8°E , 43°N) for PIE simulations, being the approximate geographical locations of the Valencia and Piedmont regions respectively (see Figs. 10 and 14 for an illustration of both domains).

The orographic data base (NGDC/NOAA of 5 minutes resolution) is linearly interpolated at the model grid points. It is subsequently smoothed by a two step filter (Shapiro, 1970) in order to avoid excessive grid-length scale orographic forcing.

Uninitialized analyses on standard pressure levels from the ECMWF, given at 00, 06, 12 and 18 UTC with a resolution of 0.75 degrees, are used to initialize the model and to supply the time-dependent boundary conditions (by a linear

interpolation between the 6 hours apart analyses). As a consequence of the spatial interpolation during the initialization process, some unbalances of the fields could arise that could induce a degradation of the forecast. In order to reduce this effect, hydrostatic balance is forced by a variational method which slightly corrects the geopotential and temperature fields across the atmospheric column, and the wind is also modified after applying a technique that minimizes the vertical integral of the horizontal divergence in order to prevent spurious gravity waves (Pinty, 1984).

For the surface submodel, we have derived a spatial distribution of seven land types for the western Mediterranean region using NOAA-AVHRR mosaics and atlas information. Such soil classification follows the table given by Benjamin and Carlson (1985). However, owing to the season in which the events occurred, the available soil moisture listed by Benjamin and Carlson has been increased by a fraction of 0.2 and 0.1 for the ALG and PIE simulations respectively. In addition, the roughness length, which is a function of soil type, has been explicitly increased in areas of elevated terrain to better represent the subgrid mountain drag (Georgelin et al., 1994). Subsoil temperature for ALG and PIE simulations corresponds to the February and November climatological values respectively, whereas sea surface temperature (kept constant during the simulation) is provided by the ECMWF surface data.

6. Simulation of Precipitation

6.1 Algeria Case

As noted in RRADS98, simulations of this case were reasonably good for the spatial pattern of precipitation in the Valencia area (exhibiting a high correlation with the coastal topography), but clearly underestimated the local maxima seen in Fig. 2. This is what experiment ALG/NC indicates (Fig. 10), which is indeed very similar to the result of experiment ALG/EM (Fig. 11). The spatial pattern of precipitation is clearly a result of the orographic lifting (Fig. 5). Both experiments show a band of important precipitation along the Valencia region extending to the north parallel to the coast, and another maximum

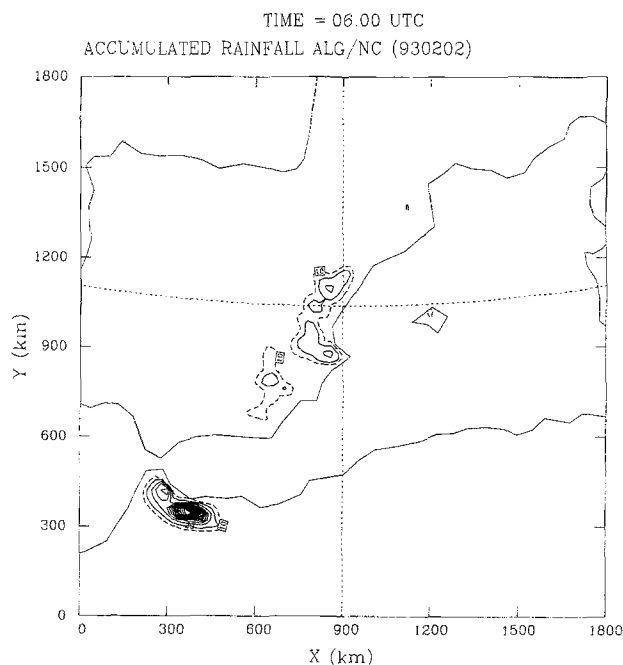


Fig. 10. Forecast total precipitation for ALG/NC experiment, accumulated from 06 UTC 1 February to 06 UTC 2 February. Contour interval is 20 mm starting at 20 mm (solid line). Dashed contour corresponds to 10 mm

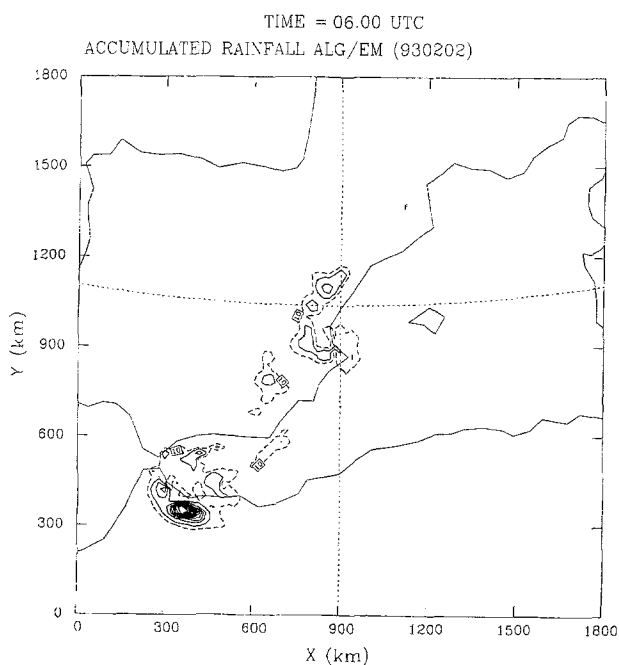


Fig. 11. As in Fig. 10 but for ALG/EM experiment

in southeastern Spain. This spatial pattern compares well with Fig. 2, except that the southern maximum occurred close to the coast and not inland as the experiments indicate. Another similitude, to be discussed further, is the strong maximum (more than 150 mm in

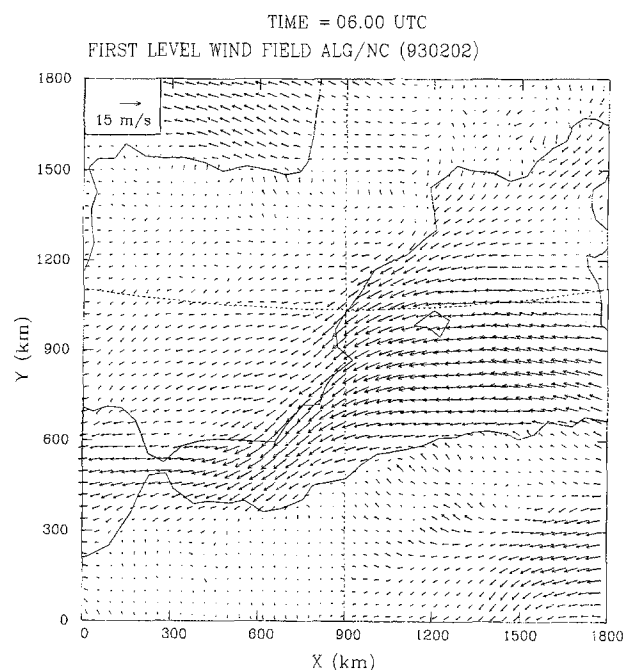


Fig. 12. Forecast surface wind field for ALG/NC experiment, on 2 February at 06 UTC. The arrow on the upper left corner represents 15 m s^{-1}

ALG/EM, and over 200 mm in ALG/NC) given in north Africa as a result of the interaction of the important coastal topography (Fig. 1) with the persistent onshore flow (Fig. 12). ALG/NC and ALG/EM only differ significantly over the sea, where the latter gives also precipitation. The forecast convective rainfall (figure not included), shows that the precipitation over the sea, where important values of CAPE occur, is entirely convective.

On the contrary, accumulated rainfall forecast by experiment ALG/KF (Fig. 13a) is substantially different from the previous ones. In this case, the precipitation band in Valencia is closer to the coast and higher quantities are obtained in its southernmost part; in southern Spain, precipitation maximums appear now close to the coast in eastern Andalusia and Gibraltar Strait as in Fig. 2, but no appreciable precipitation is obtained inland. More importantly, the convective contribution to the precipitation field is very notable in this case (Fig. 13b), not only restricted over the sea as in ALG/EM simulation, but also affecting the coastal areas. In fact, the forecast precipitation is exclusively of convective type except in the Valencia region (compare Fig. 13a,b). This result shows that ascending motion

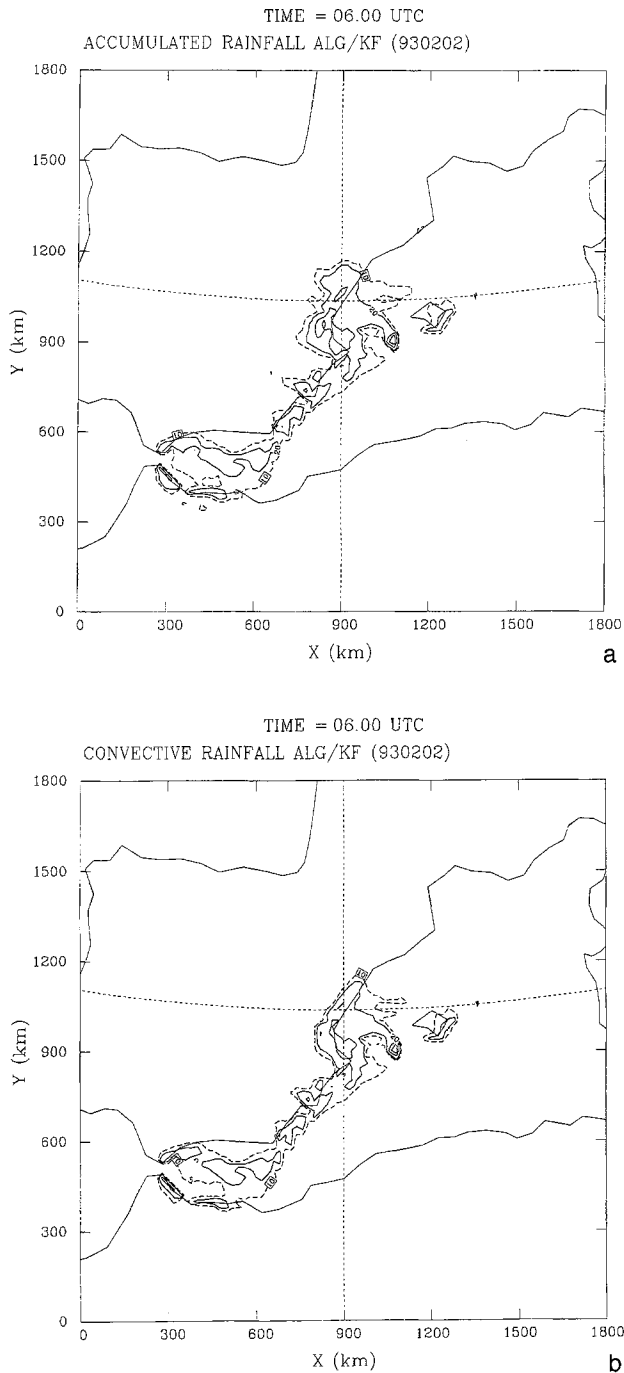


Fig. 13. Forecast precipitation for ALG/KF experiment, accumulated from 06 UTC 1 February to 06 UTC 2 February. (a) Total, (b) Convective. Contour interval is 20 mm starting at 20 mm (solid line). Dashed contour corresponds to 10 mm

associated with coastal upslope flow and with low level convergence in the sea-land transition has been an important mechanism to initiate the convection in the KF scheme.

The strong maximum in the north of Africa does not appear in this case, certainly as a result

of the discharge of air moisture and thermal stabilization produced upstream over the western Mediterranean by the important convective activity. This hypothesis will be corroborated in next section by analysing the vertical profiles.

Satellite infrared pictures of this case (Fig. 4) show convection over the sea, in agreement with simulations ALG/EM and ALG/KF, and also over the coastal zone as ALG/KF does. Undoubtedly, the images do not contain any cloud signature that could explain significant rain in the north of Africa; thus, satellite pictures support the ALG/KF result.

6.2 Piedmont Case

The fact that a significant part of the rainfall over land fell as non-convective precipitation (Lionetti, 1996; Buzzi and Tartaglione, 1996), signifies that the numerical model has a good chance of getting many of the spatial and quantitative details forecast correctly. What is needed is a reasonably accurate forecast of the low-level flow relative to the orography. This is what the model, in fact, managed to provide (RRADS98, Fig. 9). Figures 14, 15a and 16a show that the

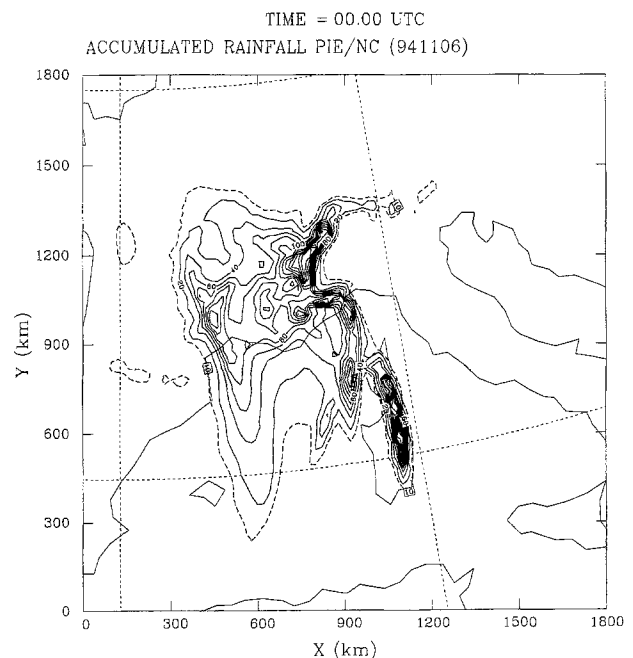


Fig. 14. Forecast total precipitation for PIE/NC experiment, accumulated from 00 UTC 5 November to 00 UTC 6 November. Contour interval is 20 mm starting at 20 mm (solid line). Dashed contour corresponds to 10 mm

observed rainfall pattern in the Piedmont area (Fig. 6) is very well predicted in all experiments, both spatially and quantitatively. Figures 15b and 16b display the role played by the convective contribution over that area, showing that the KF

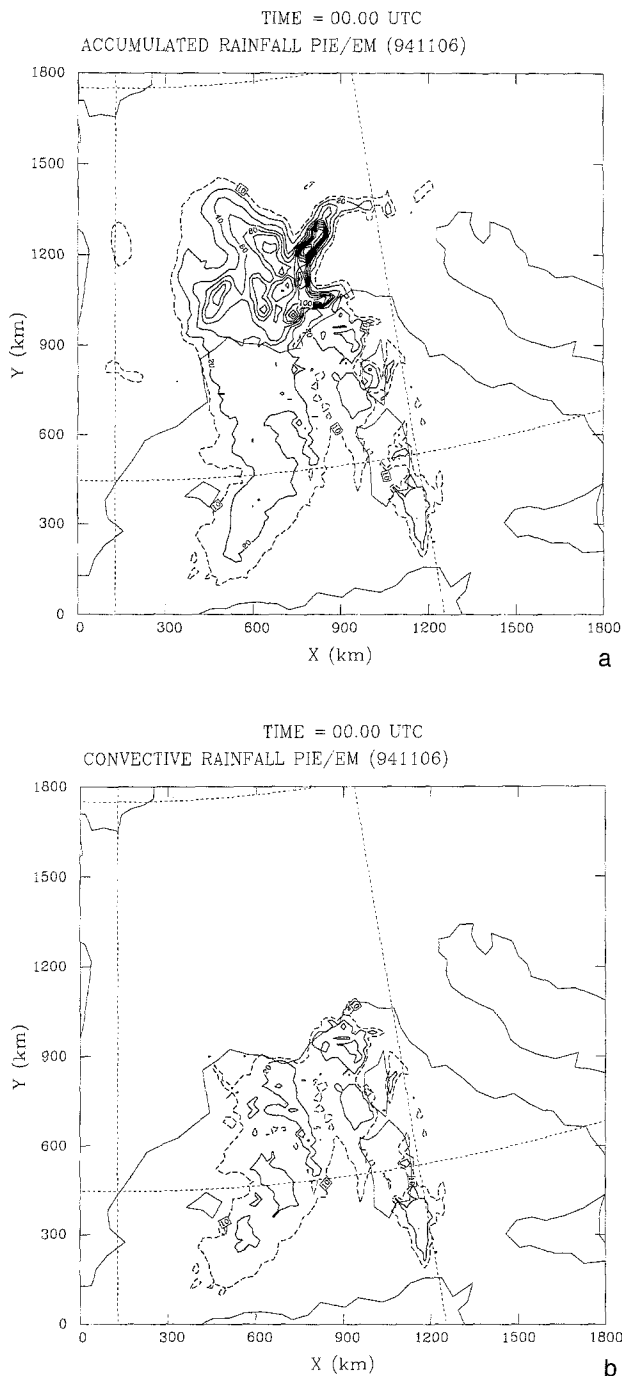


Fig. 15. Forecast precipitation for PIE/EM experiment, accumulated from 00 UTC 5 November to 00 UTC 6 November. (a) Total, (b) Convective. Contour interval is 20 mm starting at 20 mm (solid line). Dashed contour corresponds to 10 mm

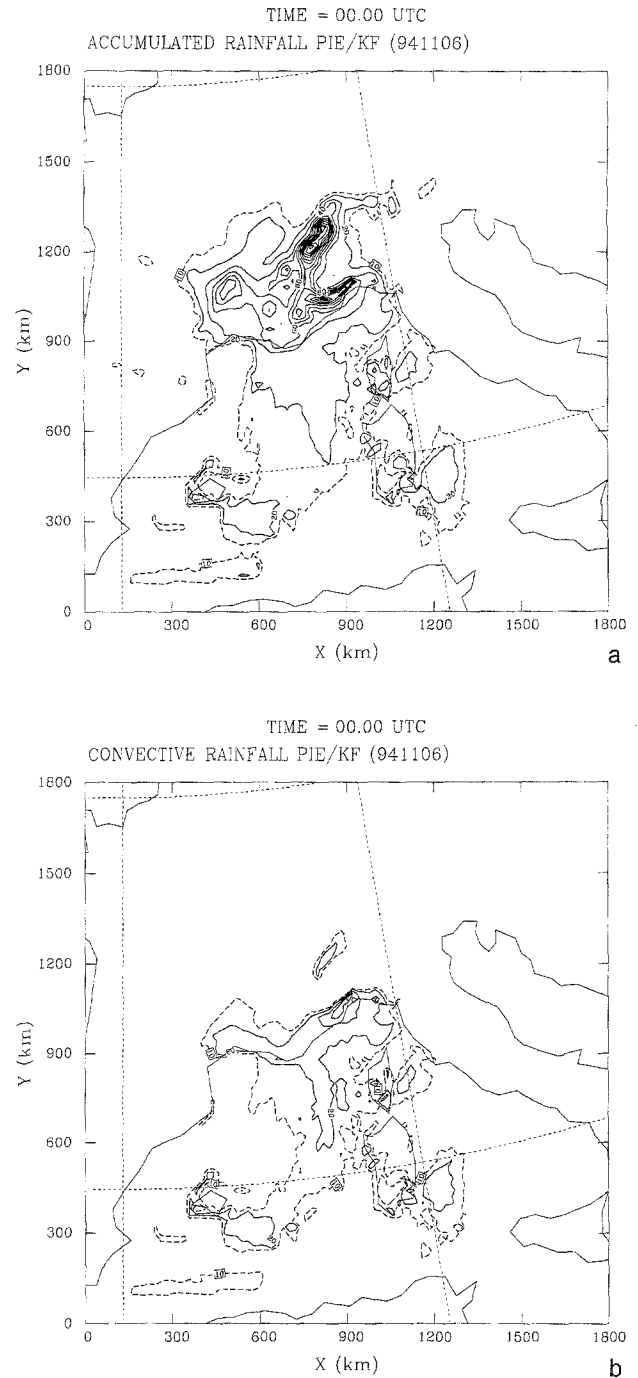


Fig. 16. As in Fig. 15 but for PIE/KF experiment

scheme contributes much more (notably in the coastal zone) than the EM scheme, as in the Algeria case. That convective activity, focused in the coastal zone, where CAPE exceeds 1000 J/kg (figure not shown), is in agreement with satellite information. Comparing Figs. 15a and 16a with 15b and 16b, it is deduced that most of the precipitation inland is essentially stratiform.

The major differences among the forecasts occur mostly over the open seas on the western Mediterranean, unfortunately where observations do not exist (except in Corsica and Sardinia, Fig. 6). All experiments show two bands of important rainfall: one, broad, just east of the Balearic Islands, and another one, narrow and still not present at 12 UTC (isohyets not shown), approximately over Corsica and Sardinia. However, in the case of the PIE/EM and PIE/KF simulations, these bands (essentially convective) take a spread shape, whereas for the PIE/NC simulation they are very intense and definite. The former structure seems more reasonable in basis of what satellite images show (Fig. 7), and agrees with observed precipitation over Corsica and Sardinia (Fig. 6). The compact bands given by PIE/NC (Fig. 14) seem to be the result of explicit convection: in the absence of parameterized convection that could act stabilizing and drying the atmosphere over wide areas, the high water vapour content condenses vigorously in localized frontal zones. In such zones, the low-level convergence can force appreciable upward velocity due to the low static stability of the air. Some soundings analysed in the next section support this scenario.

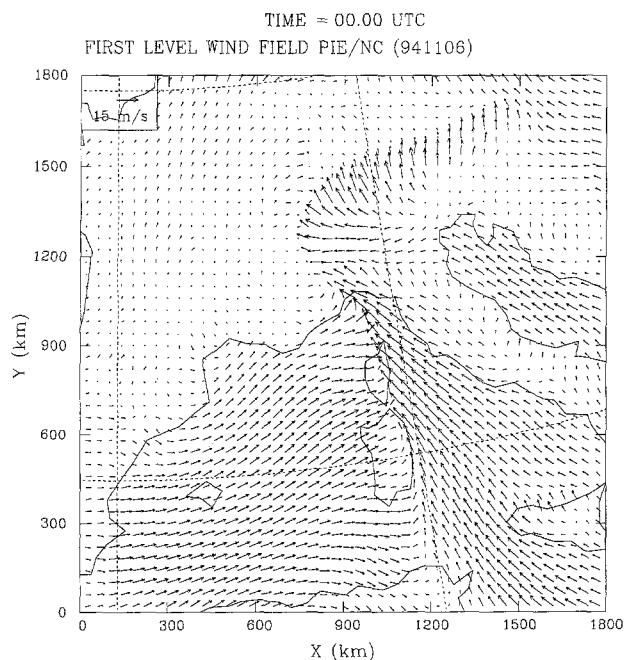


Fig. 17. Forecast surface wind field for PIE/NC experiment, on 6 November at 00 UTC. The arrow on the upper left corner represents 15 m s^{-1}

Figure 17, that corresponds to 00 UTC, shows one of these convergence lines along Corsica and Sardinia. It is responsible, probably supported by the prominent topography of the islands, for the narrow band of heavy precipitation given by the model over that area (Fig. 14). It is interesting to note that PIE/EM and PIE/KF (figures not shown) also give that convergence line, but it is appreciably smoother than in Fig. 17 and displaced farther eastward, especially in PIE/KF (about 150 km). Such more advanced position is responsible for the convective rainfall present eastward of Sardinia and Corsica in Figs. 15 and 16 (especially in the latter), and it is coherent with Fig. 7, that shows how at 18 UTC convection is already occurring between the islands axis and the Italian peninsula, and southeast of Sardinia. It seems, therefore, that the inclusion of convective parameterizations has also important consequences on the forecast wind patterns, avoiding exaggerated developments of convergence lines as that shown in Fig. 17.

7. Simulation of Temperature and Humidity Profiles

In this section, the ability of each experiment to forecast the convectively transformed air masses is quantified by comparing the observed temperature and humidity profiles with the simulated ones. For each event, we have selected some points directly affected by convection or being downstream of regions where convection occurred: PAL, MUR, VAL and AFR for the Algeria case; PAL, NIM, GEN, MIL, AJA and CAG for the Piedmont case (see Fig. 1). As observations, we take the same ECMWF analyses used to nest the model (in DRRA98, these fields were compared against real soundings and proved as high quality data).

Note from Fig. 1 that the selected points are far enough from the boundaries, so that the simulated structures are basically produced by the physics of the inner domain and little affected by the relaxation process toward the boundary 'exact' fields.

Comparison of forecast heating and drying profiles with observed values involves considerable uncertainty because the time and space scales of the physical processes responsible are

often highly disparate (recall, for instance, the 'random' nature of convection). In addition, owing to their coarser resolution, ECMWF analysis can not resolve small mesoscale structures that are possible in the mesoscale simulations. To reduce these problems, although the comparison is done at fixed times, the soundings to be compared (both simulated and 'analyzed') are calculated as spatial averages on a $200 \times 200 \text{ km}^2$ square (11×11 grid points), for each standard pressure level between 300 and 1000 hPa. The comparisons are done after 6, 18, and 30 hours of simulated time. At each time and place, we have quantified the degree of correspondence by computing the root mean square (rms) of the temperature and specific humidity errors throughout the atmospheric column.

A global measure of the performance of each scheme can be obtained by comparing the number of times the scheme performs the best (minimum rms) against the number of times it performs the worst (maximum rms). Tables 2–5 show the results of this test for each considered location.

For the Algeria case (Tables 2 and 3), results of performance reveal a clear predominance of the KF scheme for both fields, scoring 8/3 for temperature and 7/1 for specific humidity. Profiles given by NC and EM were quite similar in this case as a consequence of the little amount of convection released by EM. However, simulated humidity profiles by ALG/EM are sig-

Table 2. Summary of the rms Test of Temperature Error for the Algeria Case. In the Pairs n_f/n_l , n_f Indicates Number of Times with the first Position (minimum rms), and n_l Number of Times with the last position (maximum rms)

	ALG/NC	ALG/EM	ALG/KF
PAL	1/0	1/1	1/2
MUR	0/0	0/3	3/0
VAL	0/1	0/2	3/0
AFR	0/2	2/0	1/1
Total	1/3	3/6	8/3

Table 3. Summary of the rms Test of Specific Humidity Error for the Algeria Case. In the Pairs n_f/n_l , n_f Indicates Number of Times with the first position (Minimum rms), and n_l Number of Times with the last Position (Maximum rms)

	ALG/NC	ALG/EM	ALG/KF
PAL	0/1	1/2	2/0
MUR	0/2	1/0	2/1
VAL	0/3	3/0	0/0
AFR	0/3	0/0	3/0
Total	0/9	5/2	7/1

nificantly better than those of ALG/NC (Table 3). The same does not hold for temperature.

In the previous section, it was noted the great disparity of the forecasts with respect to the rainfall maximum in north Africa (Figs. 10, 11 and 13a). Figure 18 shows the specific humidity difference (forecast minus observed) profiles on that location. The driest sounding at all times

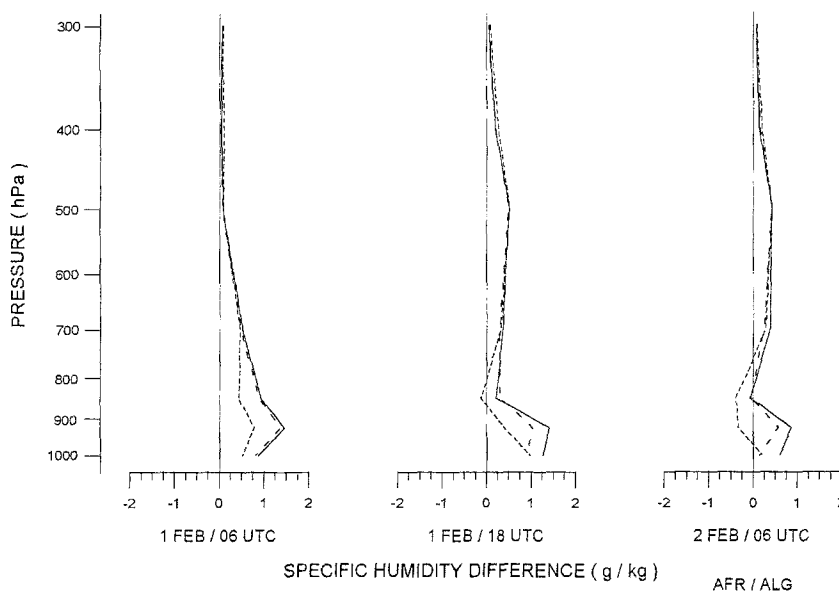


Fig. 18. Specific humidity difference profiles (forecast minus observed) at AFR (see Fig. 1), for ALG/NC (solid line), ALG/EM (long dashed), and ALG/KF (short dashed)

Table 4. As in Table 2 but for the Piedmont Case

	PIE/NC	PIE/EM	PIE/KF
PAL	2/0	0/1	1/2
NIM	0/2	1/0	2/1
GEN	0/2	0/1	3/0
MIL	0/2	1/0	2/1
AJA	0/2	1/0	2/1
CAG	0/2	2/0	1/1
Total	2/10	5/2	11/6

Table 5. As in Table 3 but for the Piedmont Case

	PIE/NC	PIE/EM	PIE/KF
PAL	0/2	1/1	2/0
NIM	0/1	0/2	3/0
GEN	1/1	0/1	2/1
MIL	3/0	0/1	0/2
AJA	0/3	1/0	2/0
CAG	2/1	1/0	0/2
Total	6/8	3/5	9/5

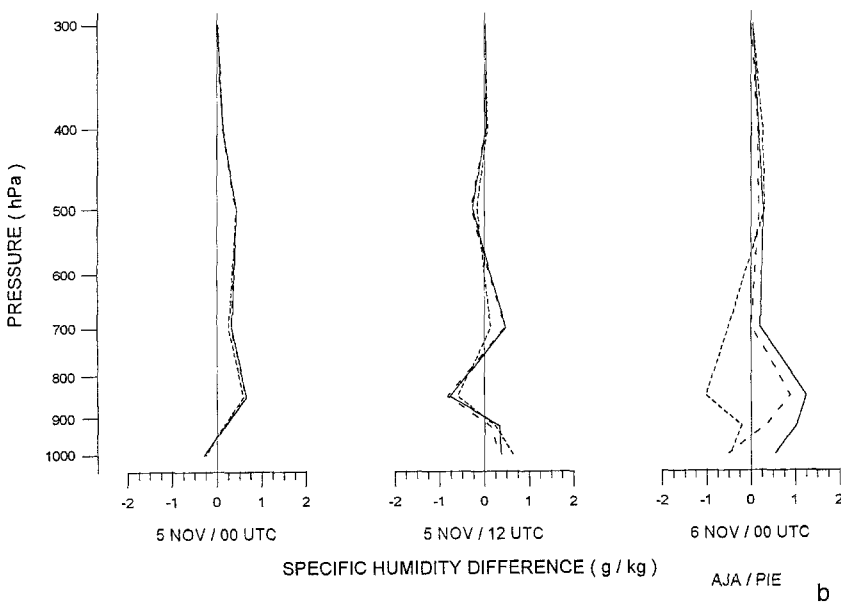
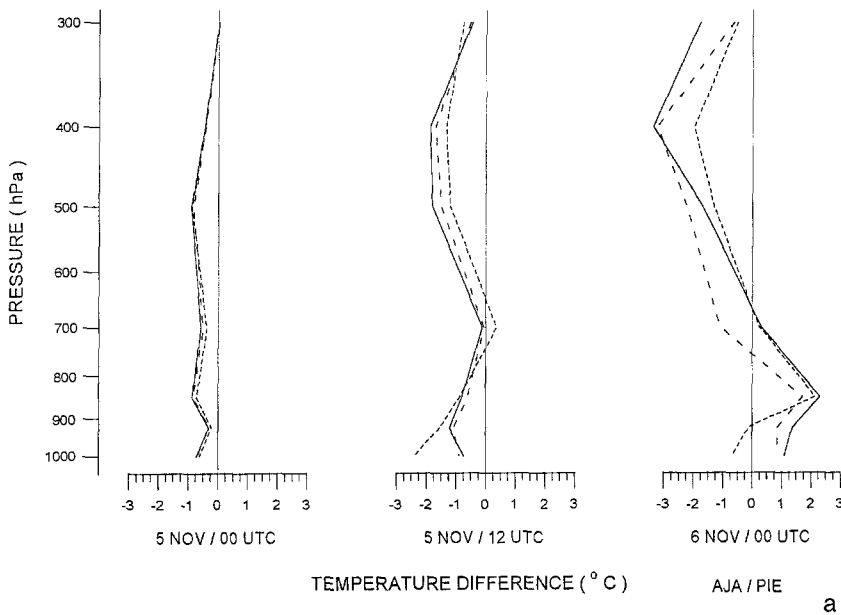


Fig. 19. Difference profiles (forecast minus observed) at AJA (see Fig. 1), for PIE/NC (solid line), PIE/EM (long dashed), and ALG/KF (short dashed). (a) Temperature, (b) Specific humidity

occurs for ALG/KF, but ALG/EM is also drier than ALG/NC. The largest disparity among the experiments is found below 700 hPa, where parcels potentially able to reach condensation are normally found. The profiles confirm the hypothesis that the convective activity that takes place upstream over the western Mediterranean dries the air sufficiently to prevent the extraordinary orographic precipitation given by ALG/NC, and in a lesser extent by ALG/EM.

For the Piedmont case (Tables 4 and 5), similar conclusions hold: PIE/EM and PIE/KF, with

scores 5/2 and 11/6 respectively, perform appreciably better than PIE/NC for temperature (the ratio being slightly in favour of PIE/EM). For humidity, PIE/KF is clearly superior, whereas PIE/EM and PIE/NC offer similar results in this case (6/8 and 3/5 respectively).

A general behaviour found in the selected soundings of this case are drier atmospheres at low levels and stabler lapse rates when a moist convection scheme has been included. This behaviour is more pronounced for PIE/KF than for PIE/EM. Figures 19 and 20 show the profiles

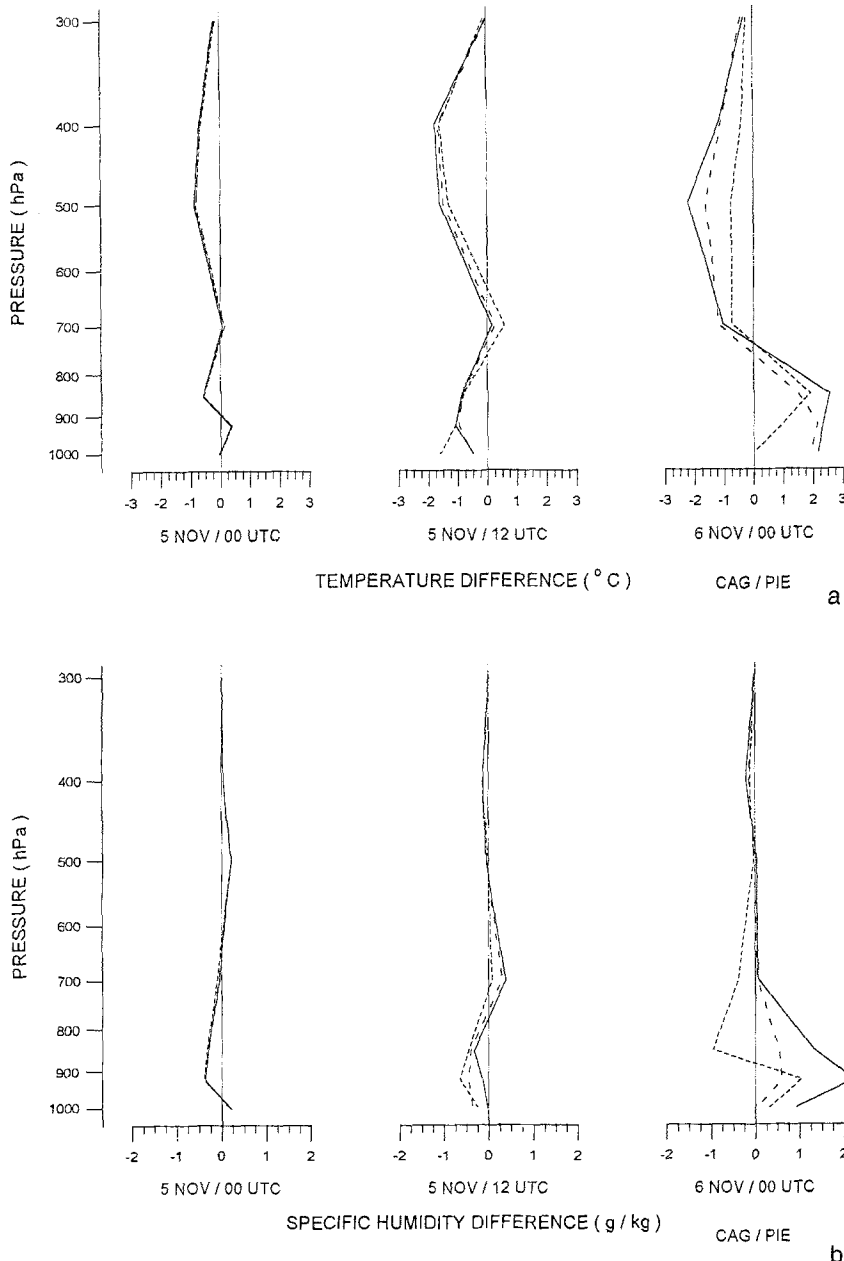


Fig. 20. As in Fig. 19 but at CAG (see Fig. 1 for location)

at AJA and CAG respectively. These locations are in Corsica and Sardinia (Fig. 1), and their atmospheric structures are especially sensitive because significant convection associated with the eastward-moving cold front occurs over the western Mediterranean. In both places, and particularly at 00 UTC on 6 November, the atmosphere obtained in PIE/KF and PIE/EM is colder at low levels and warmer at upper levels than for PIE/NC (Figs. 19a and 20a). Nevertheless, the observed lapse rates are still smaller. The atmospheres are also drier for the experiments including implicit convection (Figs. 19b and 20b), even more than the observed at some layers.

8. Conclusions

The forecast of heavy precipitation is a major challenge for mediterranean operational forecasters. With the advent of efficient computational capabilities, the strong topographic influence provides a real opportunity for successful application of meso- β scale numerical models for that task. Sensitivity of forecasts to different physical parameterizations (in their sophistication or in their closure assumptions) is a problem that must be addressed, however. This work tries to do a contribution to this subject, since the real necessity of cumulus convection parameterizations and their possible benefits have been partly delimited for two representative cases of heavy rainfall in the western Mediterranean: One case (Algeria) dominated by warm, moist advection at low levels and presenting spot convection over the sea and coastal zone; and the other (Piedmont), with a dominant frontal dynamics and presenting more organized convection over wide oceanic areas and also over the coast.

Convection of the kind embedded in maritime air masses, explosive convection forced by the coastal topography and even convection triggered by important land heating can all take place in the western Mediterranean. It would be unrealistic to expect that a certain convection scheme could respond case to case to the complex nature of convection that takes place in this region. In this work, we have applied the Emanuel (1991) and Kain and Fritsch (1990) schemes, already used for other simulations in the western Mediterranean.

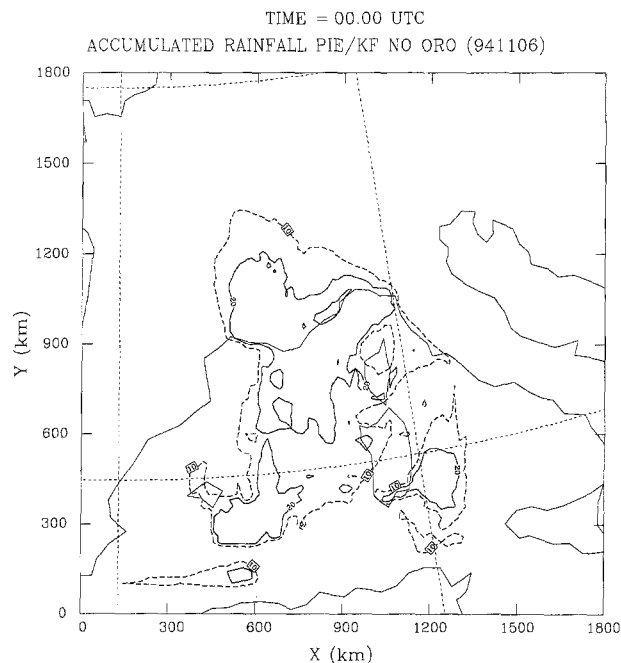


Fig. 21. Forecast precipitation for PIE/KF experiment when the orography is suppressed, accumulated from 00 UTC 5 November to 00 UTC 6 November. Contour interval is 20 mm starting at 20 mm (solid line). Dashed contour corresponds to 10 mm

The results obtained show that the strong topographic influence is the principal factor to determine the rainfall patterns and intensities over land areas. In DRRA98, it was shown that characteristic Froude numbers for both case studies imposed a 'flow over' regime (Smith, 1989), so that the coastal orography can act as an effective precipitation enhancer for impinging moist flows. In those circumstances, the merit of a good quantitative precipitation forecast (QPF) basically corresponds to the low-level flow relative to the orography. Figure 21, to be compared with Fig. 16a, shows the model-predicted rainfall by PIE/KF when the orography is suppressed. Comparing against observed rainfall (Fig. 6), it is quite clear how regardless of an appreciable synoptic and front scale forcing, an excellent forecast (Fig. 16a) can become a worthless one (Fig. 21) by solely eliminating the orographic forcing.

However, the inclusion of parameterized convection has beneficial effects on the forecast fields. A simple statistics has been carried out demonstrating that more realistic temperature and humidity profiles are obtained when using a cumulus convection parameterization. This fact

becomes determinant for precipitation and surface wind forecasts as consequence of a feedback process (presumably more remarkable as the simulation extends longer). In particular, due to the stabilization and drying rates produced by convection (preferentially over oceanic areas), artificial and intense rainfall patterns are prevented downstream where the flow is forced to ascend by topography or frontal convergence lines.

The results obtained indicate that, in principle, the Kain-Fritsch scheme performs better than the Emanuel scheme. In particular, the former seems to be more sensitive to the presence of the coastal topography, focusing convection on that area in agreement with observations. Nevertheless, extraction of general conclusions needs the simulation of more cases, and the sensitivity of each scheme to some internal adjustable parameters can not be obviated.

Acknowledgements

This work was partially supported by EC EU5V-CT94-0442, CICYT AMB95-1136-CE, and DGICYT PB94-1169-C02-02 grants. The authors sincerely acknowledge Prof. J.L. Casanovas of the University of Valladolid (Spain) for providing the Meteosat images. Precipitation data were generously provided by Spanish, French, and Italian meteorological services. The authors acknowledge two anonymous referees for their suggestions that have helped to improve the original version of the paper.

References

- Arakawa, A., Schubert, W. H., 1974: Interaction of a cumulus cloud ensemble with the large-scale environment. Part I. *J. Atmos. Sci.*, **31**, 674–701.
- Benjamin, S.G., Carlson, T.N., 1985: Some effects of surface heating and topography on the regional severe storm environment. Part I: Three-dimensional simulations. *Mon. Wea. Rev.*, **114**, 307–329.
- Berry, E. X., Reinhardt, R. L., 1973: Modeling of condensation and collection within clouds. D. R. I. Phys. Sci. Pub. No. 16. University of Nevada.
- Bhumralkar, C. M., 1975: Numerical experiments on the computation of ground surface temperature in an atmospheric general circulation model. *J. Appl. Meteor.*, **14**, 1246–1258.
- Blackadar, A. K., 1976: *Modeling the nocturnal boundary layer*. Proceedings of the Third Symposium on Atmospheric turbulence, Diffusion and Air Quality, American Meteorological Society, Boston, 46–49.
- Bougeault, P., Lacarrère, P., 1989: Parameterization of orographic induced turbulence in a mesobeta scale model. *Mon. Wea. Rev.*, **117**, 1872–1890.
- Buzzi, A., Tartaglione, N., 1996: Some aspects of the Piedmont flood: Frontal splitting and role of humid processes. *MAP Newsletter*, **5**, 38–39.
- Davies, H. C., 1976: A lateral boundary formulation for multilevel prediction models. *Quart. J. Roy. Meteor. Soc.*, **102**, 405–418.
- Doswell, C.A. III, Ramis, C., Romero, R., Alonso, S., 1998: A diagnostic study of three heavy precipitation episodes in the western Mediterranean region. *Wea. Forecasting*, **13**, 102–124.
- Emanuel, K. A., 1991: A scheme for representing cumulus convection in large-scale models. *J. Atmos. Sci.*, **48**, 2313–2335.
- Fernández, C., Gaertner, M. A., Gallardo, C., Castro, M., 1995: Simulation of a long-lived meso- β scale convective system over the mediterranean coast of Spain. Part I: Numerical predictability. *Meteorol. Atmos. Phys.*, **56**, 157–179.
- Font, I., 1983: *Climatología de España y Portugal*. Instituto Nacional de Meteorología, Apartado 285, 28071, Madrid, 296 pp.
- Frank, W. M., 1983: The cumulus parameterization problem. *Mon. Wea. Rev.*, **111**, 1859–1871.
- Fritsch, J. M., Chappell, C. F., Hoxit, L. R., 1976: The use of large scale budgets for convective parameterization. *Mon. Wea. Rev.*, **104**, 1408–1418.
- Fritsch, J. M., Chappell, C. F., 1980: Numerical prediction of convectively driven mesoscale pressure systems Part I: Convective parameterization. *J. Atmos. Sci.*, **37**, 1722–1733.
- Georgelin, M., Richard, E., Petitdidier, M., Druilhet, A., 1994: Impact of subgrid-scale orography parameterization on the simulation of orographic flows. *Mon. Wea. Rev.*, **122**, 1509–1522.
- Kain, J. S., Fritsch, J. M., 1990: A one-dimensional entraining/detraining plume model and its application in convective parameterization. *J. Atmos. Sci.*, **47**, 2784–2802.
- Kreitzberg, C. W., Perkey, D. J., 1976: Release of potential instability. Part I: A sequential plume model within a hydrostatic primitive equation model. *J. Atmos. Sci.*, **33**, 456–475.
- Lionetti, M., 1996: The Italian floods of 4–6 November 1994. *Weather*, **51**, 18–27.
- Louis, J. F., 1979: A parametric model of vertical eddy fluxes in the atmosphere. *Bound. Layer Meteor.*, **17**, 187–202.
- Maddox, R., 1980: Mesoscale convective complexes. *Bull. Amer. Meteor. Soc.*, **61**, 1374–1387.
- Mahfouf, J. F., Richard, E., Mascart, P., 1987a: The influence of soil and vegetation on the development of mesoscale circulations. *J. Climate Appl. Meteor.*, **26**, 1483–1495.
- Mahfouf, J. F., Richard, E., Mascart, P., Nickerson, E. C., Rosset, R., 1987b: A comparative study of various parameterizations of the planetary boundary layer in a numerical mesoscale model. *J. Climate Appl. Meteor.*, **26**, 1671–1695.
- Mahrer, Y., Pielke, R. A., 1977: The effects of topography on the sea and land breezes in a two-dimensional numerical model. *Mon. Wea. Rev.*, **105**, 1151–1162.
- Meteorological Office, 1962: *Weather in the Mediterranean*. Air Ministry, Vol. 1, 362 pp.

- Nickerson, E. C., Richard, E., Rosset, R., Smith, D. R., 1986: The numerical simulation of clouds, rain and airflow over the Vosges and Black forest mountain: a meso- β model with parameterized microphysics. *Mon. Wea. Rev.*, **114**, 398–414.
- Paccagnella, T., Tibaldi, S., Buizza, R., Scoccianti, S., 1992: High-resolution numerical modelling of convective precipitation over Northern Italy. *Meteorol. Atmos. Phys.*, **50**, 143–163.
- Pinty, J. P., 1984: *Une méthode variationnelle d'ajustement des champs de masse et de vent*. Note 72 de l'I.O.P.G., Université de Clermont II.
- Pinty, J. P., Mascart, P., Richard, E., Rosset, R., 1989: An investigation of mesoscale flows induced by vegetation inhomogeneities using an evapotranspiration model calibrated against HAPEX-MOBILHY data. *J. Appl. Meteor.*, **28**, 976–992.
- Ramis, C., Jansá, A., Alonso, S., Heredia, M. A., 1986: Convection over the western Mediterranean. Synoptic study and remote observation. *Rev. de Meteorología*, **7**, 59–82.
- Ramis, C., Llasat, M. C., Genovés, A., Jansá, A., 1994: The October-1987 floods in Catalonia: Synoptic and Mesoscale Mechanisms. *Meteor. Applicat.*, **1**, 337–350.
- Ramis, C., Alonso, S., Llasat, M. C., 1995: A comparative study of two cases of heavy rain in Catalonia. *Surv. in Geophys.*, **16**, 141–161.
- Ramis, C., Romero, R., 1995: A first numerical simulation of the development and structure of the sea breeze in the island of Mallorca. *Ann. Geophys.*, **13**, 981–994.
- Raymond, D. J., Blyth, A. M., 1986: A stochastic model for nonprecipitating cumulus clouds. *J. Atmos. Sci.*, **43**, 2708–2718.
- Richard, E., Mascart, P., Nickerson, E. C., 1989: The role of surface friction in downslope windstorms. *J. Appl. Meteor.*, **28**, 241–251.
- Riosalido, R., 1990: *Characterization of mesoscale convective systems by satellite pictures during PREVIMET MEDITERRANEO-89*. Segundo Simposio Nacional de Predicción. Instituto Nacional de Meteorología, Apartado 285, 28071, Madrid, 135–148.
- Romero, R., Alonso, S., Nickerson, E. C., Ramis, C., 1995: Influence of vegetation on the development and structure of mountain waves. *J. Appl. Meteor.*, **3**, 2230–2242.
- Romero, R., Ramis, C., Alonso, S., 1997: Numerical simulation of an extreme rainfall event in Catalonia: Role of orography and evaporation from the sea. *Quart. J. Roy. Meteor. Soc.*, **123**, 537–559.
- Romero, R., Ramis, C., Alonso, S., Doswell III, C. A., Stensrud, D. J., 1998: Mesoscale model simulations of three heavy precipitation events in the western Mediterranean region. *Mon. Wea. Rev.*, (in press).
- Shapiro, R., 1970: Smoothing, filtering and boundary effects. *Rev. Geophys. Space Phys.*, **8**, 359–387.
- Smith, R. B., 1989: *Hydrostatic Airflow over Mountains*. (*Advances in Geophysics*, Vol. 31) San Diego, California: Academic Press, 1–41.

Author's address: Romualdo Romero, Clemente Ramis and Sergio Alonso, Meteorology Group, Departament de Física, Universitat de les Illes Balears, Ctra. Valldemossa km 7.5, E-07071 Palma de Mallorca, Spain.